



King Saud University
Arabian Journal of Chemistry

www.ksu.edu.sa
www.sciencedirect.com



ORIGINAL ARTICLE

Theoretical evaluation of the corrosion inhibition performance of 1,3-thiazole and its amino derivatives



Lei Guo, Xiaolei Ren, Yang Zhou, Shenying Xu, Yulong Gong, Shengtao Zhang *

School of Chemistry and Chemical Engineering, Chongqing University, Chongqing, PR China

Received 12 December 2013; accepted 2 January 2015

Available online 12 January 2015

KEYWORDS

Thiazole;
Corrosion inhibitors;
Surface energy;
Density functional theory;
Molecular dynamics
simulation

Abstract The corrosion inhibition performances of three corrosion inhibitors on mild steel in acidic medium, namely 1,3-thiazole (TA), 2-amine-1,3-thiazole (2-ATA), and 4-amine-1,3-thiazole (4-ATA), were theoretically evaluated using quantum chemistry calculations and molecular dynamics simulations both in gas phase and aqueous phase. The frontier orbital energy, global activity, and Fukui indices were studied. Adsorption energy of corrosion inhibitors on iron surface was calculated. Furthermore, a prediction of iron crystal morphology was performed, and the surface energies were obtained. The results indicate that Fe (1 10) surface possesses the lowest surface energy. 4-ATA shows the highest reaction activity among the three molecules. The binding energies of the corrosion inhibitor molecules and iron surface follow the order 4-ATA > 2-ATA > TA.

© 2015 The Authors. Production and hosting by Elsevier B.V. on behalf of King Saud University. This is an open access article under the CC BY-NC-ND license (<http://creativecommons.org/licenses/by-nc-nd/4.0/>).

1. Introduction

The corrosion of metals, including mild steel, is a serious problem in many industries, especially during processes such as the pickling of steel, acid washing and etching (Makhlouf et al., 1996). One method of protecting it from corrosion is to use organic inhibitors, which are heterocyclic compounds containing P, S, O, or N and have π bonds (Obot et al., 2011; Khaled,

2010; Benabdellah et al., 2011; Abdel-Rehim et al., 2011). These hetero-atomic compounds can be seen as environmentally friendly corrosion inhibitors because of their characteristics of strong chemical activity and low toxicity. Studies reported that the inhibiting effect mainly depends on some physicochemical and electronic properties of the organic compound molecule which related to its functional groups, steric effects, π orbital character of donating electrons and electronic density of donor atoms (Finšgar and Milošev, 2010). In this regard, the effects of the molecular structure on the chemical reactivity have been a subject of great interest for research.

Interactions at metal surfaces and interfaces are critical to understand the corrosion inhibition phenomena. Properties of interest to corrosion scientists include the structure of the interface or interphase, how it differs from the bulk and the interaction of inhibitor molecules with metal surface. Due to the relatively large number of molecules (atoms) involved in

* Corresponding author at: No. 174 Shazhengjie, Shapingba, Chongqing 400044, China. Tel.: +86 023 65106756.

E-mail address: stzhcq@163.com (S. Zhang).

Peer review under responsibility of King Saud University.



Production and hosting by Elsevier

adsorption on metal surface, a molecular dynamics (MD) method using a proper force field is the best choice (Musa et al., 2012; Mesli et al., 2011). Besides, quantum chemical calculation, especially density functional theory (DFT), has also been used to analyze the characteristics of the inhibitor/surface mechanism and to describe the structural nature of the inhibitor in the corrosion process (Peljhan and Kokalj, 2011; Obi-Egbedi and Obot, 2012; Al-Mobarak et al., 2010).

Some thiazole derivatives are corrosion inhibitors with superior property and are applied widely in the protection of mild steel (Shanbhag et al., 2011; Zheludkevich et al., 2005; Quraishi et al., 2002). Whereas, to the best of our knowledge, no theoretical background has been systematically proposed to evaluate the corrosion inhibition performances of 1,3-thiazole (TA) and its amino derivatives, *i.e.*, two isomers: 4-amine-1,3-thiazole (4-ATA) and 2-amine-1,3-thiazole (2-ATA). In this paper, MD and density functional theory are employed to discuss the adsorption configuration, adsorption energy, frontier orbital energy, etc., and to explain the mechanism of above-mentioned three chemicals on iron surface in water solution or not. Therefore, we can offer more theoretical information of designing novel inhibitors.

2. Methods and definitions

2.1. Computational details

Density functional theory (DFT) calculations were carried out using the B3LYP (Becke, 1993) functional, together with the standard double-zeta plus polarization 6-311G (*d*, *p*) (Harihara and Pople, 1973) basis set implemented in the GAUSSIAN 03 software. Following the standard nomenclature the calculation will be referred to as B3LYP/6-311G**, and the frequency analysis was performed to ensure that the researched molecules reached their respective ground state. Generally, the phenomenon of electrochemical corrosion occurs in the liquid phase, so it is necessary to consider the effect of solvent in the calculations. Thus, self-consistent reaction field (SCRF) theory, with Tomasi's polarized continuum model (PCM) was applied to perform the computations in solution. This method models the solvent (water) as a continuum of uniform dielectric constant ($\epsilon = 78.54$) and defines the cavity where the solute is placed as a uniform of series of interlocking atomic spheres (Lesar and Milošev, 2009). What needs to stress, local reactivity has been analyzed by means of Fukui Indices (Parr and Yang, 1984), and these properties were calculated with DMol³ version 5.0 available in Materials Studio (Ziegler, 1991), using a BLYP (Becke exchange plus Lee–Yang–Parr correlation) functional (Hamprecht et al., 1998) and a double-numeric quality basis set with polarization functions (DND), which size is comparable with Gaussian 6-311G** basis set.

A prediction of iron crystal morphology was necessary before the simulation process. Three representative methods, *i.e.*, the Bravais–Friedel–Donnay–Harker (BFDH) method (Donnay and Harker, 1937; Prywer, 2004), the surface free-energy (SFE) model (Bisker-Leib and Doherty, 2001), and the Attachment Energy (AE) method (Hartman and Perdok, 1955), were utilized to predict crystal structures. More detailed descriptions about these models can be found in Yang and Dong (2011).

The MD simulation of the interaction between the 1,3-thiazole and its amino derivatives molecules and the Fe (110) surface was carried out in a simulation box ($2.97 \times 2.97 \times 5.05$ nm) with periodic boundary conditions in order to model a representative part of an interface devoid of any arbitrary boundary effects. Using six layers of iron atoms gives a sufficient depth that the inhibitor molecules will only be involved in non-bond interactions with iron atoms in the layers of the surface, without increasing the calculation time unreasonably. This also ensured that the depth of the surface was greater than the non-bond cutoff used in calculation. Two types of solvent layers were constructed: one consisted of 1000 H₂O molecules and a single dissolved inhibitor molecule, and the other only consisted of one inhibitor molecule.

The simulation was performed under 298 K, NVT ensemble, with a time step of 1 fs and the simulation time of 200 ps. The temperature was controlled by Andersen thermostat (Andersen, 1980). The initial velocity of each molecule accorded with Maxwell–Boltzmann distribution. Based on hypotheses, such as periodic boundary condition and equivalence of time-average and ensemble-average, Newtonian motion equations were solved with Velocity Verlet algorithm. Van der Waals and coulomb interactions were calculated by atom-based method, and the cutoff radius was 0.95 nm. During the process of simulations, all the atoms in the Fe (110) surface were fixed. COMPASS (Condensed-phase Optimized Molecular Potentials for Atomistic Simulation Studies) (Bazooyar et al., 2012) was used to optimize the structures of all components of the system of interest. It is a powerful force field supporting atomistic simulation of condensed phase materials and enables accurate and simultaneous prediction of structural, conformational, vibrational, and thermophysical properties for a broad range of molecules in isolation and in condensed phase, and under a wide range of conditions of temperature and pressure.

2.2. Definitions of global reactivity descriptors

According to density functional theory, for an *N*-electron system with total energy *E* and external potential ($v(\vec{r})$), electronegativity (χ) known as the negative of chemical potential (μ), has been defined as the first derivative of the *E* with respect to *N* at $v(\vec{r})$ (Parr et al., 1978).

$$\chi = -\mu = -(\partial E / \partial N)_{v(r)} \quad (1)$$

Hardness (η) has been defined as the second derivative of the *E* with respect to *N* at $v(\vec{r})$, which measures both the stability and reactivity of a molecule (Parr and Pearson, 1983).

$$\eta = (\partial^2 E / \partial N^2)_v = (\partial \mu / \partial N)_v \quad (2)$$

Pearson (Pearson, 1966) formulated his hard and soft acids and bases (*HSAB*) principle in the qualitative context, asserting that hard acids preferably interact with hard bases, and soft acids with soft bases. Relevant to hardness is global softness (*S*), defined as the reciprocal of the hardness: $S = 1/\eta$.

The natural way to approximate the electronic chemical potential μ and the chemical hardness η in DFT is directly evaluating from the ionization potential (*IP*) and electron affinity (*EA*) energies (Boshra et al., 2013):

$$\mu = -(IP + EA)/2 \quad (3)$$

$$\eta = (IP - EA)/2 \quad (4)$$

According to Koopman's theorem (Pearson, 1988), the energies of the HOMO and the LUMO orbitals of the inhibitor molecule are related to IP and EA , respectively, by the relationships: $IP = -E_{\text{HOMO}}$ and $EA = -E_{\text{LUMO}}$. The obtained values of η and χ were used to calculate the fraction of electrons transferred (ΔN) from the inhibitor to metallic surface as well as the initial molecule-metal interaction energy ($\Delta\psi$) by the following equations (Sastri and Perumareddi, 1997):

$$\Delta N = \frac{\chi_{\text{Fe}} - \chi_{\text{inh}}}{2(\eta_{\text{Fe}} + \eta_{\text{inh}})} \quad (5)$$

$$\Delta\psi = -\frac{(\chi_{\text{Fe}} - \chi_{\text{inh}})^2}{4(\eta_{\text{Fe}} + \eta_{\text{inh}})} \quad (6)$$

where a theoretical value of $\chi_{\text{Fe}} \approx 7$ eV is taken for iron, and $\eta_{\text{Fe}} = 0$ is taken assuming that $IP = EA$ for bulk metals, because they are softer than the neutral metallic atoms.

The global electrophilicity index (ϕ), which measures the electrophilic power of a molecule, has been given the following simple expression (Parr et al., 1999):

$$\phi = \frac{\chi_{\text{inh}}^2}{4\eta_{\text{inh}}} \quad (7)$$

3. Results and discussion

3.1. Geometries and global reactivity

The B3LYP/6-311G** fully optimized structures of two isomeric forms of amino-1,3-thiazole and of 1,3-thiazole itself

are illustrated in Table 1, where selected geometrical parameters in the gas phase and in aqueous solution, as well as the numbering of the atoms of interest necessary for discussion are given. The equilibrium bond lengths (BL), together with the bond orders (BO) for the bonds in the five member ring and the distance from the amino group to the corresponding ring atom are presented in the table. TA shows ideal planar structure of C_s symmetry. In the amino derivatives, the nitrogen atom N6 has the sp^3 hybridization. The calculated bond lengths in the gas phase and aqueous phase do not differ significantly. It can be observed that for TA, the BOs are contained in the 1.2–1.6 range. In consistency with the calculated equilibrium bond lengths, these BO values suggest a relatively strong aromatic character for the five-member ring of thiazole. Different BOs were found for 2-ATA. Two BOs are close to 1.1, implying a single bond between the sulfur and carbon (C2 and C5) atoms, while in the C2–N3–C4–C5 region, the BO ranges from 1.2 up to 1.5. This suggests a considerable delocalization of the electronic cloud in this region, that is, in 2-ATA the sulfur atom has decreased considerably the aromatic character of the ring. But we found little evidence this is happening in the 4-ATA case.

The effectiveness of an inhibitor can be related to not only its spatial molecular structure, but also with their molecular electronic structure. According to frontier orbital theory, the reaction of reactants mainly occurred on the HOMO and LUMO, and the formation of a transition state is due to an interaction between the frontier orbitals of the reactants. So, it was important to investigate the distribution of HOMO and LUMO for exploration of inhibition mechanism. Organic

Table 1 Selected geometrical parameters and Mayer bond orders of 1,3-thiazole and the amino-1,3-thiazole isomers in gas and aqueous phases.

Bond	Phase ^a	TA		2-ATA		4-ATA	
		BL (Å)	BO	BL (Å)	BO	BL (Å)	BO
S1–C2	G	1.74783	1.2518	1.77272	1.1653	1.73541	1.2904
	A	1.74344	1.2753	1.77492	1.1702	1.73327	1.3068
C2–N3	G	1.29630	1.6150	1.29975	1.5350	1.29788	1.5940
	A	1.30014	1.5888	1.30618	1.5020	1.30083	1.5689
N3–C4	G	1.37546	1.2918	1.37820	1.2671	1.37934	1.2254
	A	1.37846	1.2781	1.38117	1.2511	1.38327	1.2172
C4–C5	G	1.36250	1.5095	1.35509	1.5607	1.37406	1.3814
	A	1.36234	1.5180	1.35484	1.5723	1.37568	1.3788
C5–S1	G	1.73154	1.2785	1.75504	1.1974	1.73818	1.2608
	A	1.73159	1.2779	1.75638	1.1894	1.73897	1.2564
C2–N6	G			1.36068	1.0748		
	A			1.35352	1.1213		
C4–N6	G					1.37139	1.0511
	A					1.36875	1.0733

^a G, gas phase ($\epsilon = 1.0$); A, aqueous phase ($\epsilon = 78.5$).

substances with a higher energy level of HOMO easily donate electrons from HOMO to an empty orbital of appropriate acceptors and E_{LUMO} denotes the ability of the molecule to accept electrons. As shown in Fig. 1, all the three inhibitor molecules have similar HOMO and LUMO distributions, which were all distributed through the whole molecule. This kind of distribution favored the preferential adsorption of inhibitor on metal surface by following two fashions: one was that the unoccupied d orbitals of Fe atom accepted electrons of inhibitor molecule to form coordinate bond, the other was that the inhibitor molecule accepted electrons from Fe atom with its anti-bonding orbitals to form back-donating bond. Fig. 2 shows the correlation diagram of frontier molecular orbitals for the investigated inhibitors and their calculated HOMO–LUMO gap (ΔE). It was generally acknowledged that low values of ΔE will provide good inhibition efficiency, because the energy for removing an electron from the last occupied orbital will be low (Gece, 2008). In Fig. 2, the values of E_{HOMO} of three amino acid compounds increased in the following order: 4-ATA > 2-ATA > TA. The values of ΔE decreased in the following order: TA > 2-ATA > 4-ATA. The trend is even more marked in aqueous phase. Thus, 4-ATA has the highest E_{HOMO} and the lowest ΔE among these three thiazole compounds. Therefore, 4-ATA has the strongest interaction with iron surface and the best inhibition effect in theory.

The effectiveness of 1,3-thiazole and its amino isomers as inhibitor has been further addressed by evaluating the global reactivity parameters. These include global softness (S),

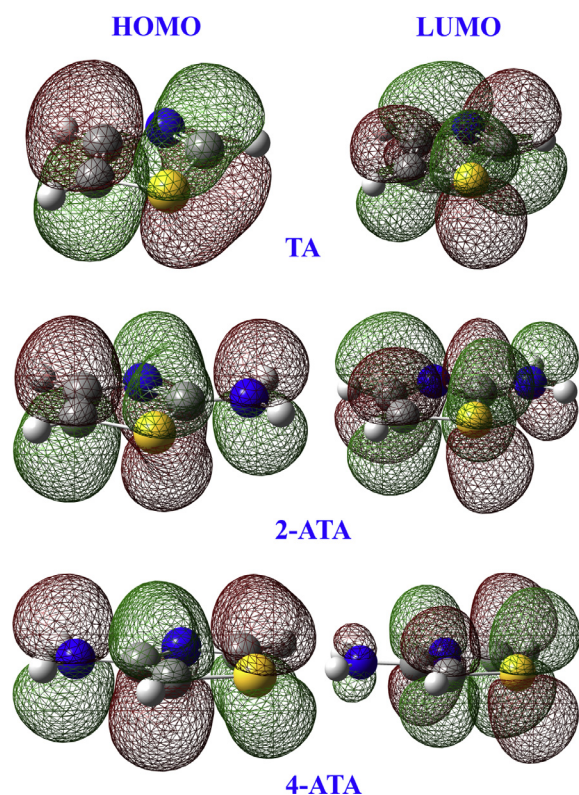


Figure 1 Schematic representation of HOMO and LUMO molecular orbital of the studied molecules (Color code: N, blue; S, yellow; C, gray; H, white; the same hereinafter).

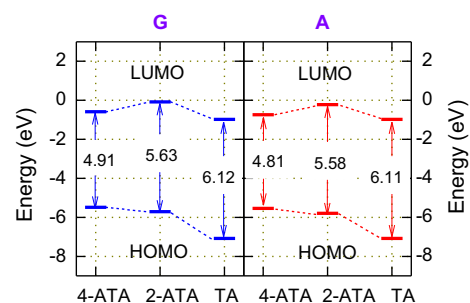


Figure 2 Correlation diagram of the frontier molecular orbitals of the inhibitors investigated, and their calculated ΔE (eV) G, gas phase ($\epsilon = 1.0$); A, aqueous phase ($\epsilon = 78.5$).

electronegativity (χ), global chemical hardness (η), global electrophilicity index (ϕ), ΔN , and $\Delta\psi$. The corresponding results are shown graphically in Fig. 3. According to *HSAB* principle, bulk metals are chemically the softest materials, this would imply that the higher is the S of inhibitor molecules the stronger is their interaction with metal surfaces. On this basis the results of Fig. 2 suggest the following trend of the inhibition effectiveness: 4-ATA > 2-ATA > TA. Furthermore, 4-ATA has the largest fraction of transferred electron to the iron metal, closely followed by 2-ATA, while the TA have the smallest value. The trend in molecule–metal interaction strength, $|\Delta\psi|$, is also 4-ATA > 2-ATA > TA. There also involves a less important descriptor to these electron-rich inhibitors, *i.e.*, global electrophilicity index; It is generally accepted that the higher the value of ϕ , the higher the capacity of the molecule to accept electrons. Compared with TA, there exists azyl ($-\text{NH}_2$) grant electron effect in 4-ATA/2-ATA, resulting in a lower value of ϕ . But when comparing the two isomers, 4-ATA displays greater efficiency in attracting electron ability, and hence the feedback bond will be strengthened. Collectively, the calculated global reactivity parameters follow the order 4-ATA > 2-ATA > TA, in agreement with the above ordering supported by electronic parameters.

Based on the data in Table 2, the PCM calculations show that the relative energies of the compounds are lower when increasing the polarity of the solvent. The solvation of the inhibitor molecules causes significant changes in the charge distribution (see Table 3, Mulliken atomic charges q), giving rise to a larger dipole moment than obtained in the gas-phase calculation. In some ways, though, the solvent effect produced small changes in the electronic structure of the inhibitor molecules, but the two phases follow the same trend for the presented properties of three molecules as discussed above. There seems to be no agreement in the literature concerning the correlation between the dipole moment and the inhibition effectiveness (Kokalj, 2010), so we did not employ the molecular dipoles to be used in a *blind* fashion to judge the inhibition effectiveness.

To describe the energy change associated with the mentioned two processes (*i.e.*, a molecule that is going to receive/back-donate a certain amount of charge), the second order simple charge transfer formula was regarded as a two-parameter expression, in which the donation and back-donation processes are differentiated through the use of the values of the chemical potential for each case, while the hardness is fixed to the value of $\eta = (\delta^+ - \delta^-)$ in both situations. Thus,

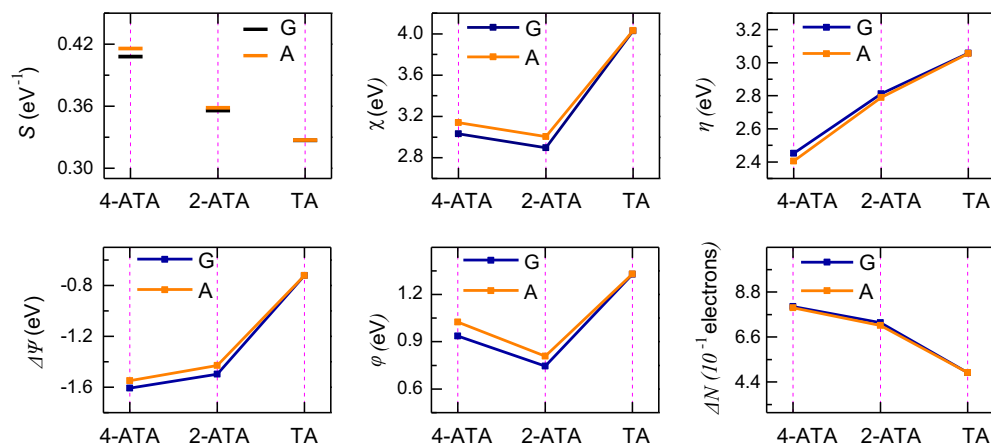


Figure 3 Calculated global reactivity parameters of 1,3-thiazole and the amino-1,3-thiazole isomers in gas phase and aqueous phase.

Table 2 Calculate total energy (T_E), total energy change (ΔE_T), and dipole moment (D) for 1,3-thiazole and the amino-1,3-thiazole isomers in gas and aqueous phases.

Inhibitor	Phase ^a	T_E (Ha)	ΔE_T (eV)	D (Debye)
4-ATA	G	-624.490	-0.613	1.543
	A	-624.497	-0.601	1.864
2-ATA	G	-624.494	-0.703	1.855
	A	-624.502	-0.697	2.543
TA	G	-569.116	-0.764	1.451
	A	-569.121	-0.763	2.008

according to the simple charge transfer model for donation and back-donation of charges proposed recently by Gomez et al. (2006) and implemented by (Obi-Egbedi et al., 2011), “when the molecule receives a certain amount of charge, ΔN^+ ,

$$\Delta E^+ = \delta^+ \Delta N^+ + 0.5\eta(\Delta N^+)^2 \quad (8)$$

while when a molecule back-donates a certain amount of charge, ΔN^- , then:

$$\Delta E^- = \delta^- \Delta N^- + 0.5\eta(\Delta N^-)^2 \quad (9)$$

If the total energy change (ΔE_T) is approximated by the sum of the ΔE^+ and ΔE^- contributions, and assuming that the amount of charge back-donated is equal to the amount of charge received, $\Delta N^- = \Delta N^+$, then:

$$\Delta E_T = \Delta E^- + \Delta E^+ = (\delta^+ - \delta^-)\Delta N^+ + \eta(\Delta N^+)^2 \quad (10)$$

The most favorable situation corresponds to the case when the total energy change becomes a minimum with respect to ΔN^+ , which implies that $\Delta N^+ = -(\delta^+ - \delta^-)/2\eta$ and that²,

$$\Delta E_T = -(\delta^+ - \delta^-)^2/4\eta = -\eta/4 \quad (11)$$

The calculations from Table 2 indicate that $\Delta E_T < 0$, thus the charge transfer to a molecule followed by back-donation from the molecule is energetically favorable. If it is assumed that the inhibition efficiency should increase when there is a better adsorption of the molecule on the metal surface, then the inhibition efficiency should increase when the stabilization energy that results from the interaction between the metal surface and inhibitor increases. As expected, the calculated ΔE_T values also exhibit the tendency: TA < 2-ATA < 4-ATA.

Table 3 Mulliken atomic charges and condensed Fukui functions for 1,3-thiazole and the amino-1,3-thiazole isomers.

Atom	Phase ^a	TA			2-ATA			4-ATA		
		q	f_k^+	f_k^-	q	f_k^+	f_k^-	q	f_k^+	f_k^-
S1	G	-0.207	0.273	0.249	-0.261	0.251	0.225	-0.225	0.263	0.223
	A	-0.195	0.280	0.230	-0.253	0.258	0.211	-0.228	0.276	0.193
C2	G	0.140	0.149	0.105	0.371	0.114	0.032	0.135	0.165	0.058
	A	0.131	0.196	0.141	0.358	0.135	0.051	0.123	0.214	0.077
N3	G	-0.284	0.098	0.078	-0.355	0.070	0.100	-0.325	0.110	0.067
	A	-0.355	0.101	0.069	-0.425	0.068	0.104	-0.383	0.115	0.064
C4	G	0.108	0.051	0.113	0.106	0.070	0.064	0.387	0.022	0.036
	A	0.087	0.070	0.161	0.078	0.100	0.093	0.362	0.036	0.060
C5	G	-0.021	0.101	0.104	-0.048	0.102	0.097	-0.123	0.091	0.102
	A	-0.032	0.132	0.145	-0.074	0.139	0.131	-0.143	0.117	0.150
N6	G				-0.366	0.066	0.130	-0.392	0.035	0.165
	A				-0.365	0.082	0.162	-0.408	0.037	0.202

^a G, gas phase ($\epsilon = 1.0$); A, aqueous phase ($\epsilon = 78.5$).

3.2. Local reactivity

The local reactivity of the inhibitors was analyzed through an evaluation of the Fukui indices, which is indicative of the reactive regions and the nucleophilic and electrophilic behavior of the inhibitor molecules. The regions of a molecule where the Fukui function is large are chemically softer than the regions where the Fukui function is small, and by invoking the *HSAB* principle in a local sense, one may establish the behavior of the different sites with respect to hard or soft reagents. For nucleophilic and electrophilic attacks, the condensed Fukui functions, f_i^+ and f_i^- , based on the finite difference approximation (Yang and Mortier, 1986), are given by:

$$f_i^+ = q_{N+1}^i - q_N^i \text{ and } f_i^- = q_N^i - q_{N-1}^i \quad (12)$$

where q_N^i , q_{N-1}^i , and q_{N+1}^i are the atomic charges on the i th atom in the neutral, cationic, and anionic species, respectively.

Although atomic charges do not have absolute meaning, they provide a crude but useful description of the electron-density distribution in molecules. In Table 3, the atomic charges derived from Mulliken analysis are given. All the nitrogen and sulfur atoms for each molecule possess an excess of negative charge. The sulfur and nitrogen atoms are assumed to play the key role for the inhibition action because these are the most negative centers of the compounds. Through comparing those Fukui indices in Table 3, it was found that the f_k^- at N6 and S1 atoms were the largest for all three molecules, which implied that these atoms preferred to provide electrons to form coordinate bonds with the metal atoms, so these atoms were the electrophilic reactive sites during absorption. As for f_k^+ , they had the larger value at C2 and C5, which implied that these atoms favored acceptance of electrons from metal atoms to form back-donating. Interestingly, S1 atom has dual characters, *i.e.*, can both donate and back-donate electrons. We hold that this has diminished its adsorption capacity since the donating process is a more important factor in evaluating local reactivity for corrosion inhibitors. Thus, from the Fukui index distribution, it could be concluded that the absorption would occur

on multiple reactivity sites, which increased adsorption stability and led to the improvement of inhibition efficiency.

3.3. Selection of adsorption surface

We calculated the surface energy (E_{surf}) in a slab model as (Arya and Carter, 2004):

$$E_{\text{surf}} = \frac{E_{\text{slab}} - (N_{\text{slab}}/N_{\text{bulk}})E_{\text{bulk}}}{2A} \quad (13)$$

where E_{slab} and E_{bulk} are the total energies of the surface slab and the bulk unit cell, respectively. N_{slab} and N_{bulk} are the number of atoms contained in the slab and the bulk unit cells, respectively, and ‘ A ’ is the area of the surface unit cell. Nine layers have been chosen to ensure the energies converge to at least 0.01 J m^{-2} . The calculated surface energies, as well as the morphology results for iron crystal are listed in Table 4. Additionally, a more intuitive micromorphology comparison diagram is produced, as shown in Fig. 4. Looking at the calculated crystal morphology of iron, you will notice the (110) face accounts for at least 63% of the crystal surface, and the most 100% in the BFDH model. The calculated surface energies increase in the following sequence: (110) < (200) < (222). This trend coincides exactly with previous theoretical results of (Arya and Carter, 2003).

Just for an added delineation, the XRD pattern of α -Fe was obtained by using the Powder Diffraction function in Reflex module included in software Materials Studio, and shown in Fig. 5. In general, the half width (FWHM) of X-ray diffraction is used as a strength index of material surface. It can be seen from Fig. 5 that the value of FWHM increases gradually as diffraction angle increases; the (110) diffraction peak possesses good intensity and then high orientation and crystallinity.

In brief, the density packed (110) surface has the most stabilization, so we choose Fe (110) surface to simulate the adsorption process.

Table 4 Surface energies and morphology results for α -Fe crystal.

hkl	Multiplicity			% Total facet area			Surface energy (J m^{-2})	
	BFDH	AE	SFE	BFDH	AE	SFE	This work	Ref. Arya and Carter (2003)
(110)	12	12	12	100	88.4	63.31	2.78	2.28
(200)	6	6	6	–	11.6	24.38	2.98	2.30
(222)	8	8	8	–	–	12.29	3.11	2.58

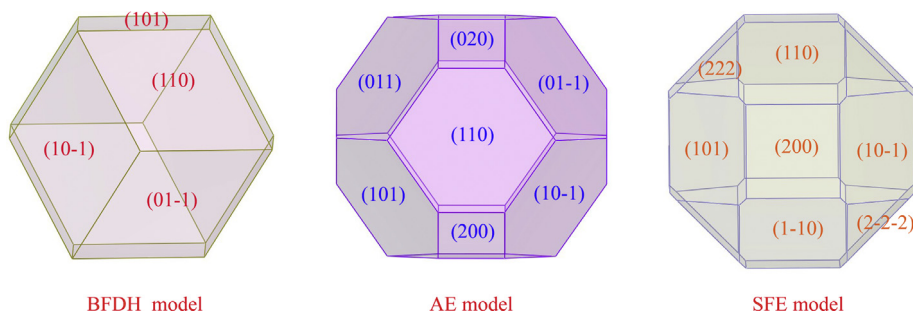


Figure 4 The crystal habits of iron simulated by three different models.

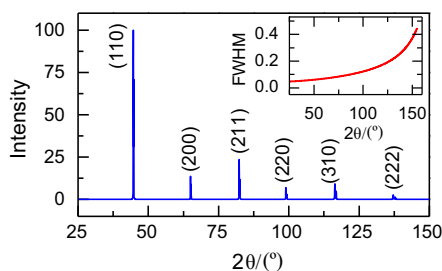


Figure 5 Simulated XRD pattern of α -Fe (Inset: FWHM vs 2theta) (X-ray, copper radiation, step size: 0.05°).

3.4. Molecular dynamics simulations

The molecular dynamics simulations were performed to study the adsorption behavior of the TA, 2-ATA, and 4-ATA on the Fe (110) surface. Whether the model system has reached equilibrium or not was ascertained by the equilibrium criterions of temperature and energy simultaneously (Zeng et al., 2011), *i.e.*, the fluctuations of temperature and energy should be confined to 5–10%. Taking 4-ATA as an example, according to the temperature and energy curves from MD simulations at 298 K (Fig. 6), the temperature fluctuates in a range of (298 ± 20) K and the fluctuation of energy is less than 0.5%, indicating that the system has reached an equilibrium state.

The equilibrium configurations for the three corrosion inhibitors are shown in Fig. 7. By careful examination of Fig. 7, it can be noticed that, during the process of simulation, 1,3-thiazole and its derivatives molecules moved gradually near the Fe (110) surface. After the system reached equilib-

rium, all the investigated inhibitors adsorbed nearly parallel to the Fe (110) surface, and they adsorb on the metal surface through the nitrogen (N) and sulfur (S) atoms as well as the five-membered aromatic rings. Quantitative appraisal of the interaction between each molecule and the Fe surface was achieved by calculating the adsorption energy (E_{ads}) using Eq. (14) (Znini et al., 2012)

$$E_{\text{ads}} = E_{\text{complex}} - (E_{\text{Fe}} + E_{\text{inh}}) \quad (14)$$

where E_{complex} is the total energy of the surface and inhibitor, E_{Fe} and E_{inh} is the total energy of the iron crystal and free inhibitor molecule, respectively. And the binding energy is the negative value of the interaction energy, $E_{\text{binding}} = -E_{\text{ads}}$. The values of the adsorption and binding energies of the three inhibitors on Fe (110) surface are listed in Table 5. The calculated values of E_{ads} are -361.83 , -307.59 , and -144.01 kJ mol $^{-1}$ for 4-ATA, 2-ATA, and TA, respectively.

Table 5 Adsorption and binding energies (all in kJ mol $^{-1}$) between the three inhibitors and Fe (110) surface.

Inhibitor	Phase ^a	E_{ads}	E_{binding}
4-ATA	G	-361.83	361.83
	A	-444.96	444.96
2-ATA	G	-307.59	307.59
	A	-392.94	392.94
TA	G	-144.01	144.01
	A	-184.03	184.03

^a G, in *vacuum*; A, in *aqueous* solution.

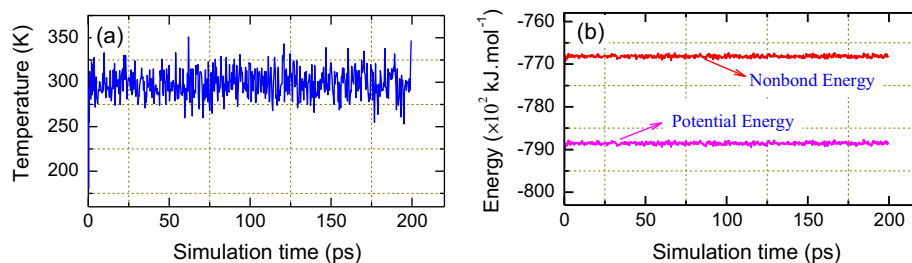


Figure 6 Temperature equilibrium curve (a) and energy fluctuant curve (b) of 4-ATA molecule on Fe (110) surface (results in *vacuo*).

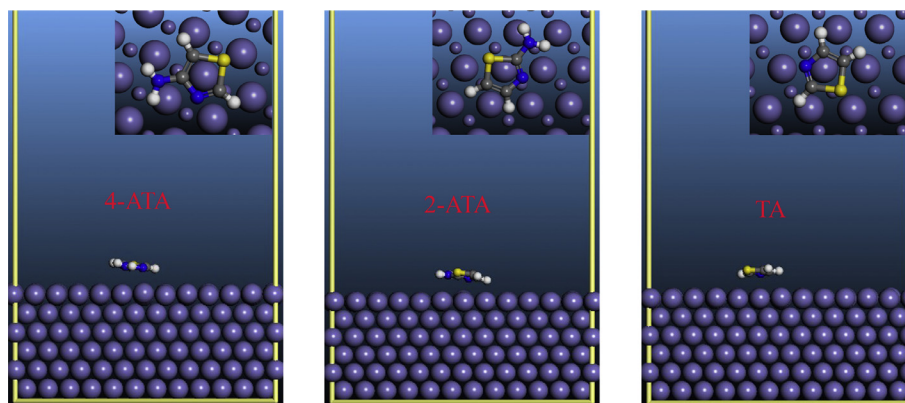


Figure 7 Representative snapshots of TA, 2-ATA, and 4-ATA on the metal surfaces, viewed along different perspectives (inset, on-top view) to support a spatial impression.

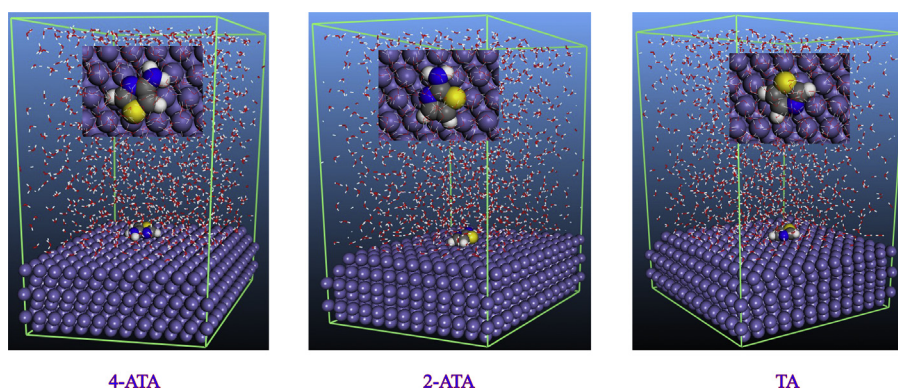


Figure 8 Equilibrium adsorption configurations of the three inhibitors on Fe (110) surface in water solution (Inset, on-top view).

The high negative values of the adsorption energies indicate that the adsorption of inhibitors on Fe (110) surface is spontaneous, strong, and stable. The binding energies are found to increase in the order $4\text{-ATA} > 2\text{-ATA} > \text{TA}$. 4-ATA gives the maximum binding energy during the whole simulation process, which indicates that 4-ATA will adsorb more strongly on the iron surface and possess better inhibition performance than the other inhibitors. This result is consistent with the aforementioned quantum chemistry analysis.

To get proper visualization of the surface orientation of the inhibitor molecules, we have modified the Fe slabs by reducing the diameters of the sub-surface Fe atoms (see Fig. 7 insets). In this case, it is especially obvious that those polarizable atoms (C, N, S) along the molecular backbone seem to avoid contact with the Fe atoms on the surface plane {larger spheres on the Fe (110) slab} and appear to align with vacant sites on the *fcc* lattice atop the metal surface. In another word, the molecular backbone of the adsorbate molecule is preferentially accommodated in characteristic epitaxial grooves on the metal surface. Such epitaxial adsorption orientations are associated with a minimum free energy of adsorption as the adsorbates can be considered as extensions of the *fcc* lattice and adsorption strength scales with improved fit of the polarizable atoms of a molecule to multiple epitaxial sites (Heinz et al., 2009). This phenomenon accounts for the high adsorption strengths of the adsorbent/adsorbate systems and is commonly seen in other corrosion inhibitors (Oguzie et al., 2011; Mejeha et al., 2012).

In order to simulate the realistic situation, it is important to take the effect of solvent into account. The corresponding simulation result is presented in Fig. 8, and the calculated interaction energy and binding energy are also listed in Table 5. It can be seen from Fig. 8 that the optimization configurations of 1,3-thiazole and its amino derivatives in aqueous solution are similar to those in the vacuum systems. Moreover, the order of E_{ads} obtained from calculations in the aqueous solution is the same as the one in the nonaqueous system. Nevertheless, the values of E_{binding} in aqueous solution are slightly higher than those in the nonaqueous system. The parallel adsorption configurations under different environments ensure that the iron surface can be maximally covered by the investigated inhibitor molecules and form a barrier layer between the iron surface and the aggressive media, thus enhancing the inhibition efficiency.

After analyzing the MD simulation results of corrosion inhibitors with iron crystal surface, pair correlation functions

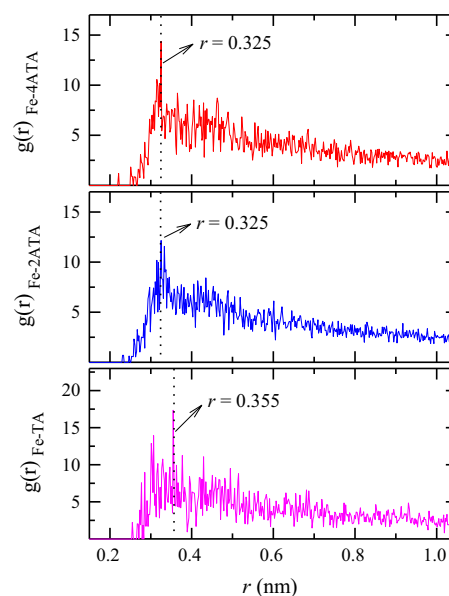


Figure 9 Pair correlation functions of the three inhibitors on Fe (110) surface in water solution.

of the super-molecular structures, $g(r)$, were obtained (see Fig. 9). As a basic rule, the peak in the $g(r) \sim r$ curve within 0.35 nm is caused by chemical bonds, and that outside 0.35 nm is caused by coulomb and Van der Waals interactions (Zeng et al., 2011). As shown in Fig. 9, the distance between the 4-ATA/2-ATA and the iron atoms of the Fe (110) face is 0.325 nm, less than 0.350 nm, which indicates that chemical bonds have formed between these two corrosion inhibitors and iron atoms. However, the Fe-TA distance (0.355) slightly exceeds 0.350 nm, suggesting a weak chemisorption. Furthermore, the countless decentralized peaks located outside 0.35 nm, which are derived from physical interactions, may also contribute to the net molecule surface attraction.

4. Conclusions

Molecular modeling was used to evaluate the structural, electronic and reactivity parameters of thiazoles in relation to their effectiveness as corrosion inhibitors. The inhibitory properties of 1,3-thiazole and its two isomeric amino derivatives were

studied by means of density functional theory, the B3LYP/6-311G** method. Quantum chemical parameters such as E_{HOMO} , E_{LUMO} , ΔE , D , η , χ , S and ΔN were given. Molecular dynamics simulations were performed to study the adsorption behavior of the inhibitors on the Fe (110) surface and it was observed that the adsorption occurs mostly through the lone pair of electrons of the hetero-atoms and π -electrons of the thiazole moiety. All values of adsorption energies, E_{ads} , are negative, which means that the adsorption could occur spontaneously. Ultimately, the values of binding energy, frontier orbital energy and energy gap indicate that corrosion inhibition efficiency was organized in the following sequences: 4-ATA > 2-ATA > TA.

Acknowledgments

This work was supported by Natural Science Foundation of China (No. 21376282), and Chongqing Graduate Student Research Innovation Project (No. CYB14019).

References

- Abdel-Rehim, S.S., Khaled, K.F., Al-Mobarak, N.A., 2011. Corrosion inhibition of iron in hydrochloric acid using pyrazole. *Arab. J. Chem.* 4 (3), 333–337.
- Al-Mobarak, N.A., Khaled, K.F., Hamed, M.N.H., Abdel-Azim, K.M., Abdelshafi, N.S., 2010. Corrosion inhibition of copper in chloride media by 2-mercapto-4-(p-methoxyphenyl)-6-oxo-1,6-dihydropyrimidine-5-carbonitrile: electrochemical and theoretical study. *Arab. J. Chem.* 3 (4), 233–242.
- Andersen, H.C., 1980. Molecular-dynamics simulations at constant pressure and-or temperature. *J. Chem. Phys.* 72 (4), 2384–2393.
- Arya, A., Carter, E.A., 2003. Structure, bonding, and adhesion at the TiC(100)/Fe(110) interface from first principles. *J. Chem. Phys.* 118 (19), 8982–8996.
- Arya, A., Carter, E.A., 2004. Structure, bonding, and adhesion at the ZrC(100)/Fe(110) interface from first principles. *Surf. Sci.* 560 (1–3), 103–120.
- Bazooyar, F., Momany, F.A., Bolton, K., 2012. Validating empirical force fields for molecular-level simulation of cellulose dissolution. *Comput. Theor. Chem.* 984, 119–127.
- Becke, A.D., 1993. Density-functional thermochemistry. 3. The role of exact exchange. *J. Chem. Phys.* 98 (7), 5648–5652.
- Benabdellah, M., Tounsi, A., Khaled, K.F., Hammouti, B., 2011. Thermodynamic, chemical and electrochemical investigations of 2-mercapto benzimidazole as corrosion inhibitor for mild steel in hydrochloric acid solutions. *Arab. J. Chem.* 4 (1), 17–24.
- Bisker-Leib, V., Doherty, M.F., 2001. Modeling the crystal shape of polar organic materials: prediction of urea crystals grown from polar and nonpolar solvents. *Cryst. Growth Des.* 1 (6), 455–461.
- Boshra, A., Bagheri, S., Jadidi, S., 2013. Global reactivity of heterostructure Armchair BC2N-(4,4) nanotubes: a density functional theory investigation. *Heteroatom Chem.* 24 (3), 168–173.
- Donnay, J.D.H., Harker, D., 1937. A new law of crystal morphology extending the law of bravais. *Am. Min.* 22 (5), 446–467.
- Finšgar, M., Milošev, I., 2010. Inhibition of copper corrosion by 1,2,3-benzotriazole: a review. *Corros. Sci.* 52 (9), 2737–2749.
- Gece, G., 2008. The use of quantum chemical methods in corrosion inhibitor studies. *Corros. Sci.* 50 (11), 2981–2992.
- Gomez, B., Likhanova, N.V., Dominguez-Aguilar, M.A., Martinez-Palou, R., Vela, A., Gazquez, J.L., 2006. Quantum chemical study of the inhibitive properties of 2-pyridyl-azoles. *J. Phys. Chem. B* 110 (18), 8928–8934.
- Hamprecht, F.A., Cohen, A.J., Tozer, D.J., Handy, N.C., 1998. Development and assessment of new exchange-correlation functionals. *J. Chem. Phys.* 109 (15), 6264–6271.
- Harihara, P.c., Pople, J.A., 1973. Influence of polarization functions on molecular-orbital hydrogenation energies. *Theoret. Chim. Acta* 28 (3), 213–222.
- Hartman, P., Perdok, W.G., 1955. On the relations between structure and morphology of crystals. 1. *Acta Crystallogr. A* 8 (1), 49–52.
- Heinz, H., Farmer, B.L., Pandey, R.B., Slocik, J.M., Patnaik, S.S., Pachter, R., Naik, R.R., 2009. Nature of molecular interactions of peptides with gold, palladium, and Pd–Au bimetal surfaces in aqueous solution. *J. Am. Chem. Soc.* 131 (28), 9704–9714.
- Khaled, K.F., 2010. Experimental, density function theory calculations and molecular dynamics simulations to investigate the adsorption of some thiourea derivatives on iron surface in nitric acid solutions. *Appl. Surf. Sci.* 256 (22), 6753–6763.
- Kokalj, A., 2010. Is the analysis of molecular electronic structure of corrosion inhibitors sufficient to predict the trend of their inhibition performance. *Electrochim. Acta* 56 (2), 745–755.
- Lesar, A., Milošev, I., 2009. Density functional study of the corrosion inhibition properties of 1,2,4-triazole and its amino derivatives. *Chem. Phys. Lett.* 483 (4–6), 198–203.
- Makhlof, M.T., ElShatory, S.A., ElSaid, A., 1996. The synergistic effect of halide ions and some selected thiols as a combined corrosion inhibitor for pickling of mild steel in sulphuric acid solution. *Mater. Chem. Phys.* 43 (1), 76–82.
- Mejeha, I.M., Nwandu, M.C., Okeoma, K.B., Nnanna, L.A., Chidiebere, M.A., Eze, F.C., Oguzie, E.E., 2012. Experimental and theoretical assessment of the inhibiting action of *Aspilia africana* extract on corrosion aluminium alloy AA3003 in hydrochloric acid. *J. Mater. Sci.* 47 (6), 2559–2572.
- Mesli, F., Mahboub, R., Mahboub, M., 2011. Molecular dynamics comparative study of methane–nitrogen and methane–nitrogen–ethane systems. *Arab. J. Chem.* 4 (2), 211–222.
- Musa, A.Y., Jalgham, R.T.T., Mohamad, A.B., 2012. Molecular dynamic and quantum chemical calculations for phthalazine derivatives as corrosion inhibitors of mild steel in 1M HCl. *Corros. Sci.* 56, 176–183.
- Obi-Egbedi, N.O., Obot, I.B., 2012. Adsorption behavior and corrosion inhibitive potential of xanthene on mild steel/sulphuric acid interface. *Arab. J. Chem.* 5 (1), 121–133.
- Obi-Egbedi, N.O., Obot, I.B., El-Khaiary, M.I., 2011. Quantum chemical investigation and statistical analysis of the relationship between corrosion inhibition efficiency and molecular structure of xanthene and its derivatives on mild steel in sulphuric acid. *J. Mol. Struct.* 1002 (1–3), 86–96.
- Obot, I.B., Obi-Egbedi, N.O., Eseola, A.O., 2011. Anticorrosion potential of 2-mesityl-1H-imidazo[4,5-f][1,10] phenanthroline on mild steel in sulfuric acid solution: experimental and theoretical study. *Ind. Eng. Chem. Res.* 50 (4), 2098–2110.
- Oguzie, E.E., Li, Y., Wang, S.G., Wang, F.H., 2011. Understanding corrosion inhibition mechanisms-experimental and theoretical approach. *RSC Adv.* 1 (5), 866–873.
- Parr, R.G., Donnelly, R.A., Levy, M., Palke, W.E., 1978. Electronegativity – density functional viewpoint. *J. Chem. Phys.* 68 (8), 3801–3807.
- Parr, R.G., Pearson, R.G., 1983. Absolute hardness – companion parameter to absolute electronegativity. *J. Am. Chem. Soc.* 105 (26), 7512–7516.
- Parr, R.G., Von Szentpaly, L., Liu, S.B., 1999. Electrophilicity index. *J. Am. Chem. Soc.* 121 (9), 1922–1924.
- Parr, R.G., Yang, W.T., 1984. Density functional-approach to the frontier-electron theory of chemical-reactivity. *J. Am. Chem. Soc.* 106 (14), 4049–4050.
- Pearson, R.G., 1966. Langford, Ch – ligand substitution processes. *Science* 154 (3746), 254.
- Pearson, R.G., 1988. Absolute electronegativity and hardness – application to inorganic-chemistry. *Inorg. Chem.* 27 (4), 734–740.
- Peljhan, S., Kokalj, A., 2011. DFT study of gas-phase adsorption of benzotriazole on Cu(111), Cu(100), Cu(110), and low coordinated defects thereon. *Phys. Chem. Chem. Phys.* 13 (45), 20408–20417.

- Prywer, J., 2004. Explanation of some peculiarities of crystal morphology deduced from the BFDH law. *J. Cryst. Growth* 270 (3–4), 699–710.
- Quraishi, M.A., Ahmad, S., Venkatachari, G., 2002. Corrosion inhibition of mild steel in boiling hydrochloric acid by some thiazole derivatives. *Bull. Electrochem.* 18 (9), 399–402.
- Sastri, V.S., Perumareddi, J.R., 1997. Molecular orbital theoretical studies of some organic corrosion inhibitors. *Corrosion* 53 (8), 617–622.
- Shanbhag, A.V., Venkatesha, T.V., Prabhu, R.A., Praveen, B.M., 2011. Inhibition effects of acetyl coumarins and thiazole derivatives on corrosion of zinc in acidic medium. *B. Mater. Sci.* 34 (3), 571–576.
- Yang, L., Dong, Y., 2011. Crystal morphology study of N,N'-diacetylchitobiose by molecular dynamics simulation. *Carbohydr. Res.* 346 (15), 2457–2462.
- Yang, W., Mortier, W.J., 1986. The use of global and local molecular-parameters for the analysis of the gas-phase basicity of amines. *J. Am. Chem. Soc.* 108 (19), 5708–5711.
- Zeng, J.P., Zhang, J.Y., Gong, X.D., 2011. Molecular dynamics simulation of interaction between benzotriazoles and cuprous oxide crystal. *Comput. Theor. Chem.* 963 (1), 110–114.
- Zheludkevich, M.L., Yasakau, K.A., Poznyak, S.K., Ferreira, M.G.S., 2005. Triazole and thiazole derivatives as corrosion inhibitors for AA2024 aluminium alloy. *Corros. Sci.* 47 (12), 3368–3383.
- Ziegler, T., 1991. Approximate density functional theory as a practical tool in molecular energetics and dynamics. *Chem. Rev.* 91 (5), 651–667.
- Znini, M., Majidi, L., Bouyanzer, A., Paolini, J., Desjobert, J.M., Costa, J., Hammouti, B., 2012. Essential oil of *Salvia aucheri mesatlantica* as a green inhibitor for the corrosion of steel in 0.5 M H₂SO₄. *Arabian Journal of Chemistry* 5 (4), 467–474.